JOURNAL OF CATALYSIS 112, 229–249 (1988)

Hydrogenation and Hydrodesulfurization over Sulfided Ruthenium Catalysts

I. Catalysts Containing Partial Monolayers of Adsorbed Sulfur

YEONG-JEN KUO AND BRUCE J. TATARCHUK[1]

Department of Chemical Engineering, Auburn University, Auburn, Alabama 36849

Received June 6, 1987; revised February 10, 1988

Thiophene hydrodesulfurization (HDS), 1-hexene hydrogenation, and 1-hexene isomerization have been investigated over sulfided $Ru/\gamma\text{-}Al_2O_3$ catalysts (1.8–10 nm crystallites) and $CoMo/\gamma\text{-}Al_2O_3$ catalysts using a differential microreactor operated at 101 kPa from 548 to 623 K. Catalysts were presulfided in 101 kPa of 10% H_2S/H_2 at $T \leq 673$ K or in 101 kPa of 100% H_2S at $T \leq 523$ K such that sulfided ruthenium catalysts retained ca. 0.25 monolayer of adsorbed sulfur. Structure-sensitive adsorption of sulfur was observed using microgravimetry and pulse oxygen chemisorption. Crystallites of 1.8 nm retained 0.1 monolayer of strongly bound sulfur while crystallites greater than 3.2 nm retained 0.25 monolayer. Sulfur adatoms produced virtual ruthenium cations with high isomerization activity while the structure-sensitive adsorption of sulfur provided for an "apparent structure sensitivity" in the hexene hydrogenation rate. This anomalous result could be reconciled by counting sulfur-free ruthenium atoms using pulse oxygen adsorption. Thiophene HDS over sulfided ruthenium catalysts proceeded via direct hydrogenolysis in the absence of tetrahydrothiophene formation. Ruthenium crystallites of 1.8 nm possessed specific activities 23 times greater than those found over 10-nm crystallites. The higher specific activity found over small ruthenium crystallites during HDS was attributed to the multiatomic ensemble requirements of the reaction, the high activity associated with a "clean metal" surface, and the greater number of "clean metal sites" found on smaller crystallites. Both 1-hexene hydrogenation and thiophene HDS were well represented by Langmuir–Hinshelwood rate expressions in which apparent activation energies, adsorption equilibrium constants, and heats of adsorption were found to depend on the ruthenium crystallite size. Sulfided Ru/Al_2O_3 (1.8-nm) catalysts provided ca. 13-fold higher 1-hexene hydrogenation rates than $CoMo/Al_2O_3$ catalysts when compared per square meter of active area, while specific 1-hexene hydrogenation rates were similar when compared per oxygen titratable site. Sulfided Ru/Al_2O_3 (1.8-nm) catalysts provided ca. 2-fold higher thiophene HDS rates than $CoMo/Al_2O_3$ catalysts when compared per square meter of active area, while specific thiophene HDS rates were ca. 7-fold higher over $CoMo/Al_2O_3$ catalysts than over Ru/Al_2O_3 when compared per oxygen titratable site.

INTRODUCTION

Sulfided forms of $CoMo/\gamma\text{-}Al_2O_3$, $NiMo/\gamma\text{-}Al_2O_3$, and $NiW/\gamma\text{-}Al_2O_3$ are commercially used as hydrotreating and *hydrodesulfurization* (HDS) catalysts due to their high dispersion and high activity per unit volume, relatively low cost, tolerance to sulfur poisons, and high specific activities for removing oxygen-, nitrogen-, and sulfur-containing functional groups and/or heteroatoms. The ability of these catalysts to process light petroleum feeds has proven so effective in the past that little incentive has existed to develop improved catalyst materials. The growing necessity to process heavier crudes, however, coupled with the eventual replacement of these materials by coal- and shale-derived synthetic crudes, provides a significantly more challenging set of catalytic requirements than those required to process lighter feeds.

In response to the above-noted realization, recent studies of both an experimental and a theoretical nature have demonstrated that other transition metal sulfides, includ-

[1] To whom all correspondence should be addressed.

0021-9517/88 $3.00

ing ruthenium sulfide (RuS_2), possess sigficantly higher specific activities toward the hydrodesulfurization of dibenzothiophene than either unpromoted molybdenum sulfide or tungsten sulfide (*1–3*). In recognition of these findings we have undertaken a number of investigations aimed at discerning the structure, stability, and catalytic mechanisms operative over sulfided ruthenium catalysts. The *objective* of these efforts has been to develop an enhanced understanding of the "structure–activity relationships" possessed by these highly active catalysts with the hope that such understandings may provide insights into the enhanced promotion and/or development of improved catalytic materials.

Results obtained in this laboratory and discussed herein demonstrate from the prospectives provided by various catalytic reactions and characterization studies that the performance of sulfided ruthenium catalysts can be classified into two distinct regimes depending on the amount of sulfur and manner in which it is incorporated onto/into the catalyst. In the first regime (e.g., produced by sulfidization in 101 kPa of 10% H_2S/H_2, ca. <723 K), less than one-half monolayer of sulfur is deposited onto the catalyst surface, which selectively catalyzes the direct hydrogenolysis of thiophene to C_4 products and H_2S in the absence of *t*etra*h*ydro*t*hiophene (THT). In the second regime (e.g., produced by sulfidization in 101 kPa of >80% H_2S/H_2, ca. >673 K), multilayers of sulfur are incorporated into the ruthenium surface with crystalline RuS_2 apparently extending all the way to the gas phase in the absence of surface crystallographic relaxations. These RuS_2-like surfaces produce nearly equal quantities of direct C_4 hydrogenolysis products and THT. Since the surface structures noted above *are stable under reaction conditions* and provide vastly different and in some cases highly desirable catalytic selectivities (hydrogenolysis versus hydrogenation), we have further focused our studies on developing a detailed understanding of the "structure–activity" and "structure–selectivity" properties provided within each sulfidization regime.

As a result of the aforementioned sulfidization regimes we have divided our studies into two distinct parts. In this paper we consider the physical and chemical characteristics of ruthenium surfaces containing *partial* monolayers of adsorbed sulfur. In the second paper (*4*) we examine the structure–reactivity behavior of thiophene HDS observed following extensive sulfidization of supported ruthenium catalysts. Results of those studies are contrasted with the data presented in this paper and utilized to provide insights into the unique and unexpected thermodynamic constraints required to form RuS_2 at the surface. Since interconversion between the two sulfidization regimes is readily accomplished, the sulfided ruthenium catalysts discussed in this and the subsequent paper appear to provide adjustable hydrogenation to hydrogenolysis activities, allowing alteration of product selectivity and efficient use of process hydrogen during HDS. The possibility also exists that results observed in these studies may be applicable at pressures greater than 101 kPa and/or for reaction systems involving the removal of oxygen and nitrogen heteroatoms.

EXPERIMENTAL

1. Catalyst Materials

Supported ruthenium catalysts in the form of 0.5, 2.0, 3.7, and 5.0% Ru/Al_2O_3 specimens were prepared, according to procedures described in detail elsewhere (*5, 6*). Aqueous solutions of $RuCl_3$–$3H_2O$ (Aesar, 99.9%) were added in a dropwise fashion to a γ-Al_2O_3 support (Harshaw A1-3945, 234 m^2/g) until incipient wetness was achieved (ca. 0.68 cm^3/g). These specimens were then dried in air for 12 h at 353 K and stored for further use. A commercial 5.0% Ru/Al_2O_3 catalyst was also used (Engelhard, Lot 118-7-FF-40, BET surface area of 120 m^2/g).

TABLE 1

Catalyst Description and Properties

	Catalyst	Ruthenium[a] crystallite size (nm)	Ruthenium[a] surface area (m^2/g)
a.	0.5% Ru/Al_2O_3[b]	1.8	0.98
b.	2% Ru/Al_2O_3	3.0	2.73
c.	2% Ru/Al_2O_3	3.2	2.56
d.	2% Ru/Al_2O_3[c]	5.3	1.55
e.	2% Ru/Al_2O_3[c]	9.8	0.84
f.	3.7% Ru/Al_2O_3	2.5	6.06
g.	3.7% Ru/Al_2O_3[c]	3.8	4.00
h.	5% Ru/Al_2O_3	3.0	6.83
i.	5% Ru/Al_2O_3[d]	5.0	4.10
j.	5% Ru/Al_2O_3[c]	6.4	3.20
k.	5% Ru/Al_2O_3[c]	9.1	2.25
l.	Ru sponge	—	0.65[e]
m.	Ru sponge	—	6.50[e]

[a] Ruthenium crystallite sizes and surface areas determined by H_2 chemisorption at 298 and 373 K prior to sulfidization. Crystallite size and surface area have been corrected for the number of sites blocked by adsorbed chlorine, where applicable, according to the procedures of Lu and Tatarchuk (*5, 6*).

[b] Chlorine, 0.17 wt% (Galbraith).

[c] Larger diameter cyrstallites obtained by sintering in sequential H_2, O_2, H_2 environments.

[d] Commercial catalyst obtained from Engelhard (Lot 118-7-FF-40). Chlorine, 0.52 wt% (Galbraith).

[e] Surface area also determined by BET methods.

Unsupported ruthenium sponges were obtained from Aesar (0.65 m^2/g, 99.5% purity) and from Engelhard (6.5 m^2/g, >96.0% purity). Surface areas determined by the BET method showed close agreement to those provided by irreversible hydrogen chemisorption measurements at 373 K.

A commercial $CoMo/\gamma$-Al_2O_3 catalyst, supplied by American Cyanamid (HDS-1442A H-Coal), was also studied for comparison purposes. This catalyst was supplied in the form of 0.50 × 0.16-cm cylindrical extrudates with loadings of 14.78% MoO_3 and 3.46% CoO, a pore volume of 0.72 cm^3/g, a bulk density of 0.32 g/cm^3, and a BET surface area of 331 m^2/g after crushing and sieving between 20 and 40 mesh.

Prior to reaction and chemisorption studies all catalysts were pressed at 1.4×10^4 kN/m^2 and sieved between 20 and 40 mesh. Properties of the catalysts are shown in Table 1. Further details of catalyst preparation and characterization procedures have been discussed elsewhere (*5–11*).

2. Chemical Reagents

Hydrogen and helium (99.99%) were obtained from Selox, Inc. and purified prior to reaction and adsorption studies by sequential passage through a Deoxo unit at 298 K, a copper turning trap at 500 K, and a bed of 13× zeolites at 77 K. Oxygen used for catalyst sintering (99.99%, from Selox, Inc.) was purified using 13× zeolites at 196 K while nitrogen for BET studies (99.99%, Linde, Inc.) was purified using a copper turning trap at 500 K and a bed of 13× zeolites at 77 K. Mixed gases including 10.2% H_2S in H_2 (99.97% overall purity) and 9.87% O_2 in He (99.99% overall purity) were supplied by Air Products (custom mixture grades) and used without further purification. Pure hydrogen sulfide (>99.5%, Matheson), as well as thiophene and 1-hexene (Aldrich), was examined by gas chromatography (>99% purity) and used without further purification.

3. Catalyst Characterization

A. Chemisorption

Volumetric hydrogen adsorption measurements were performed in an all-Pyrex apparatus described previously (*5, 6*). Measurements of the number of surface ruthenium atoms per gram of catalyst and estimates of the resultant crystallite size were determined primarily on the basis of irreversible hydrogen uptakes measured at 373 K.

Average crystallite diameters determined from hydrogen adsorption data are reported on a "prior to sulfidization basis" since recent work performed in this laboratory (*8–12*) has indicated that as little as 0.25 monolayer of adsorbed sulfur is sufficient

to block irreversible hydrogen adsorption onto ruthenium surfaces at temperatures between 77 and 473 K.

Because 0.25 monolayer of sulfur adatoms precludes irreversible hydrogen adsorption, pulse oxygen chemisorption was used to measure the number of vacant ruthenium surface sites following various sulfidization treatments. For these studies, catalyst samples were loaded into a 2.2-mm-i.d. stainless-steel U-tube and placed onto a pulse adsorption apparatus. Following reduction and/or presulfidization at 673 K, catalysts were purged at this temperature with pure helium at a flow rate of 50 cm^3/min for 1 h. The effluent from the U-tube was then routed over the thermal conductivity detector of a gas chromatograph (Gow-Mac, 69-150) and the O_2 uptake measured at 298 K. Pulses of 10% O_2/He were added to the He carrier (i.e., 1.09 μmole O_2/pulse) at 30-s intervals until successive oxygen peaks increased by less than 1%.

Mean crystallite sizes and available ruthenium surface areas reported for catalysts used during kinetic studies were assumed to be the same as those determined within the various adsorption apparatuses, on catalysts from the same precursor batch, following identical reduction/pretreatment procedures. The role of these adsorption measurements is to compliment data obtained by kinetic and gravimetric studies and to provide a basis for the calculation of specific activity.

B. Micrograviметry

A Cahn 2000 microbalance with a capacity of 1.5 g and an ultimate precision of ± 0.2 μg was employed to determine the amount of sulfur incorporated into/onto unsupported ruthenium catalysts following various sulfidization treatments. Details of the equipment are given by Moran (*13*) and Bowers (*14*).

Prior to sulfidization, 0.65 m^2/g ruthenium samples were reduced at 673 K for 8 h inside the hang down tube, purged at 673 K in helium or argon for 1.5 h, cooled in the purge gas to room temperature, evacuated, and the base weight was recorded. Samples were subsequently exposed to H_2S/H_2 mixtures (10–100% H_2S, 298–823 K) for varying times, purged at reaction temperatures for 1.5 h, brought to room temperature in the purge gas, evacuated, and a new weight was recorded. Since sulfidization did not significantly change the surface areas of these specimens, the amount of sulfur retained by the catalyst has been expressed on a monolayer equivalent basis where one monolayer of sulfur corresponds to one sulfur adatom per surface ruthenium atom prior to sulfidization. The number of surface ruthenium atoms present was determined by buoyancy-corrected BET isotherms assuming that the cross section of the nitrogen molecule is 0.162 nm^2 and the average area per surface ruthenium atom is 0.0817 nm^2 (*15, 16*).

4. Kinetic Studies

A. Reactor System

A flow reactor system with extensive mixing of gases (viz., H_2S, H_2) and liquid reactants (viz., thiophene or 1-hexene) was employed. Liquid reactants were fed from a 5-cm^3 Hamilton "gas/liquid-tight" syringe using a Harvard syringe pump and entered into a thermostated vaporization section. The vaporized liquid reactants were mixed with H_2S and H_2 controlled by Linde mass flow controllers and fed to a 400-cm^3 mixing volume. The mixture was then routed through two 6-port-2 position gas sampling valves (Valco) equipped with 0.25-cm^3 sampling loops. The mixture could be sampled on each side of the reactor by appropriate valve positioning. All connecting lines located after the vaporization section were maintained at 393 ± 10 K to prevent condensation of products and reactants.

Two different reactors were used depending on the catalyst loading and/or the reaction being studied. One vessel, a down-

flow quartz reactor, was used when a charge of between 2 and 20 g of catalyst was required. The other reactor, a 3.2-mm-i.d. stainless-steel tube, was employed when less than 2 g of catalyst was required. Temperature control in all instances was held within ±2 K by Lindberg ovens surrounding the vaporization and reactor sections.

B. Reaction Conditions

Thiophene hydrodesulfurization and 1-hexene hydrogenation were performed over the temperature range from 548 to 623 K with a catalyst charge varying from 49 mg to 16 g. Partial pressures of thiophene, 1-hexene, hydrogen, and hydrogen sulfide were varied in the following ranges: thiophene, 5.35–18.5 kPa; 1-hexene, 2.73–12.83 kPa; H_2, 85.6–112.1 kPa; H_2S, 1.01–10.1 kPa. Unless specified otherwise, hydrogen sulfide was always present in these feeds to prevent changes in surface structure due to sulfur depletion by process hydrogen. Reactants were introduced at the desired rate and the system was allowed to reach steady state (ca. 8 h) as demonstrated by constant conversions measured in successive reactant and product samplings. No evidence for permanent deactivation or slow activity decline was observed after this induction period.

C. Analysis of Products and Reactants

Reactants and products were analyzed using a Varian 3700 gas chromatograph equipped with a thermal conductivity detector. For thiophene studies, glass columns 3.6 m in length and 2 mm i.d. were packed in their first 1.8 m with 80–100 mesh Chromosorb 107 (Alltech) and in the latter 1.8 m with 3% Sp-2250 on 100–120 mesh Supelcoport (Supelco Inc.). A 333 to 473 K temperature interval, ramped at 10 K/min, was sufficient to separate H_2, H_2S, butene, butane, thiophene, tetrahydrothiophene, and small amounts of cracking products observed in this study. In the case of 1-hexene hydrogenation, 3.0-m × 3.2-mm-i.d. stainless-steel columns were used and packed with 10% tricresylphosphate on 60–80 mesh Chromosorb W (Varian Corp.). These columns, operated isothermally at 303 K, allowed separation of H_2, H_2S, 1-hexene, and hexane, as well as the sequential isomerization products of *cis*- and *trans*-2-hexene followed by *cis*- and *trans*-3-hexene.

D. Reactor Model

Thiophene hydrodesulfurization and 1-hexene hydrogenation were carried out at low conversions (0.5–10%) allowing a steady-state differential model to be employed. Differential operation was required to permit discrimination of primary and secondary products while permitting accurate measurements of the intrinsic reaction rate extrapolated to zero conversion.

Percentages of thiophene HDS conversions were calculated on the basis of the number of moles of thiophene converted divided by the number of moles of thiophene in the reactant feed; similarly, 1-hexene hydrogenation conversions were determined based on the number of moles of hexane produced divided by the number of moles of 1-hexene in the reactant feed. Details of the calculations of thiophene HDS and 1-hexene conversions are described elsewhere (*9–11*).

E. Kinetic Models Evaluated

A number of generalized Langmuir–Hinshelwood rate expressions based on the following form were evaluated as candidates to correlate observed rate data,

$$-r_i = \frac{k_i P_i P_{H_2}^a}{(1 + K_i P_i + K_S P_S)^b (1 + K_{H_2} P_{H_2})^c}, \quad (1)$$

where k_i is the apparent rate constant for reactant i (1-hexene or thiophene), K_i is the adsorption equilibrium constant of component i (1-hexene or thiophene), P_i is the pressure of component i (1-hexene or thiophene), H_2 is hydrogen, S is hydrogen

sulfide, and *a, b, c,* are constants (0, 1, and 2 were evaluated).

A nonlinear least-squares regression analysis based on the method of Marquardt (*17*) was used to fit the data. The goodness of fit for different rate equations was determined by comparing the residual sum of squares for the differences observed between experimental and computed rates at 95% confidence levels.

F. Catalyst Pretreatment Prior to Kinetic Studies

$CoMo/Al_2O_3$ catalysts were loaded into the tubular reactor, flushed with He for 2 h at 473 K and presulfided at 673 K in 10% H_2S/H_2 (50 cm^3/min (STP)) for 2 h. Following presulfidization, catalysts were cooled to reaction temperatures in 10% H_2S/H_2; the H_2S/H_2 stream was then diluted to ca. 1% H_2S/H_2 before a coreactant (i.e., thiophene or 1-hexene) was introduced.

Ru/Al_2O_3 catalysts of 0.5, 2.0, 3.7, and 5.0% loading as well as unsupported ruthenium sponges were reduced in 50 cm^3/min (STP) of flowing H_2 for 8 h followed by *mild presulfidization* treatments involving either (i) 50 cm^3/min of 1 to 10% H_2S in H_2 at 101 kPa for varying times at temperatures below 673 K or (ii) 50 cm^3/min of 100% H_2S at 101 kPa for varying times at temperatures below 523 K.

TABLE 2

Comparison of Pulse O_2 and Static H_2 Chemisorption Uptakes on "Clean" Ru/Al_2O_3 Catalysts

Catalyst	d (nm)[a]	O_2 uptake at 298 K (μmole/g)	H_2 uptake[a] at 298 K (μmole/g)	Ratio of (O_2/H_2)
0.5% Ru/Al_2O_3	1.8	4.51	7.94	0.57
5% Ru/Al_2O_3	3.0	30.8	54.06	0.57
2% Ru/Al_2O_3	5.3	12.5	22.5	0.55
5% Ru/Al_2O_3	9.1	8.2	15.3	0.54
$CoMo/Al_2O_3$[b]	—	85.0	—	—

[a] Calculations based on the H_2 uptake at 298 K following excursion in adsorption temperature to 373 K (*5, 6*). Reported diameter accounts for sites blocked by chlorine adatoms and assumes (i) one hydrogen atom per surface ruthenium atom, (ii) cubic crystallites with five sides exposed, and (iii) 0.0817 nm^2 per surface ruthenium atom; see Refs. (*5, 6*) for more details.

[b] Commercial $CoMo/Al_2O_3$ catalyst from American Cyanamid (HDS-1442A H-Coal); BET surface area, 331 m^2/g.

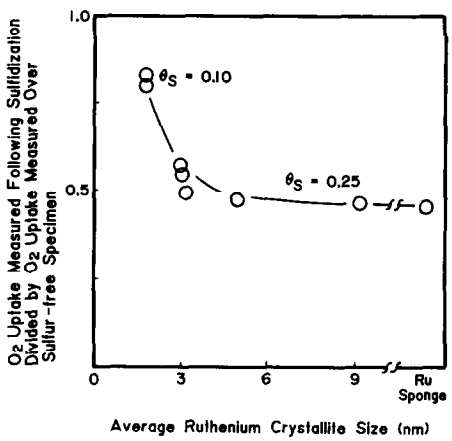

FIG. 1. Effect of Ru crystallite size on the ratio of pulse O_2 uptakes measured at 298 K before and after sulfidization in 10% H_2S/H_2, 101 kPa, 673 K, 2 h.

RESULTS

1. CATALYST CHARACTERIZATION

A. Microgravimetry

Microgravimetric studies performed on 0.65 m^2/g ruthenium sponge catalysts revealed that the number of incorporated sulfur atoms to the number of surface ruthenium atoms, prior to sulfidization, increased with increasing temperature, hydrogen sulfide concentration, and sulfidization time. While this general trend is not suprising, it is noteworthy in the context of this study that sulfidization at 673 K in 101 kPa of 10% H_2S/H_2, for periods as short as 1 min or as long as 1 week, provided stationary uptake ratios of ca. 0.3 (viz., $S_{(a)}/Ru_{(s)} = 0.3$).

B. Oxygen and Hydrogen Chemisorptions

Results of oxygen and hydrogen chemisorption measurements performed over a number of 0.5–5.0% Ru/Al_2O_3 catalysts before and after sulfidization are shown in Table 2 and Fig. 1. Over reduced Ru/Al_2O_3 catalysts (i.e., sulfur-free specimens), pulse

oxygen uptakes at 298 K are approximately one-half the value measured by static hydrogen adsorption methods (Table 2). Since hydrogen atoms are known to adsorb with a 1 : 1 surface stoichiometry to clean ruthenium surface atoms under these conditions (*18, 19*), the data of Table 2 suggest that pulse oxygen adsorption at 298 K saturates at approximately one oxygen atom for every two surface ruthenium atoms.

After sulfidization in 101 kPa of 10% H_2S/H_2 at 673 K for 2 h, oxygen uptakes decreased significantly compared to those uptakes measured from reduced (i.e., sulfur-free) Ru/Al_2O_3 specimens (see Fig. 1). Irreversible hydrogen uptakes were found to be completely poisoned at adsorption temperatures between 77 and 473 K (see Part II (*4*) of this series for details).

In contrast to the data shown in Table 2, Fig. 1 now provides apparent evidence for structure-sensitive adsorption of oxygen following sulfidization. Crystallites larger than 3.2 nm lose about one-half their adsorption capacities toward oxygen, whereas crystallites below 3.2 nm appear to be increasingly more difficult to poison, losing only about 20% of their oxygen adsorption sites.

2. Kinetic Measurements

A. *Verification of Reactor Model*

Differential reaction conditions were obtained at low conversions as shown in Fig. 2. This behavior was verified each time a new catalyst was loaded. The absence of inter- and intraparticle gradients under reaction conditions was checked according to the methods of Satterfield (*20*) and Mears (*21*). The modified Thiele moduli for thiophene HDS and 1-hexene hydrogenation were found to be 2.1×10^{-3} and 2.4×10^{-2}, respectively, giving rise to effectiveness factors close to 1 under reaction conditions. Therefore, it has been assumed that measured reaction rates were not limited by either heat or mass transfer.

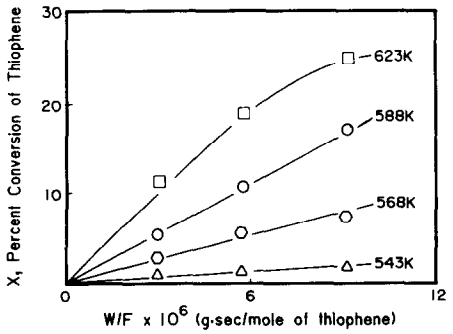

FIG. 2. Demonstration of differential reaction conditions for 0.3 g of 5% Ru/Al_2O_3. Feed: 9.33% thiophene, 0.87% H_2S, and 89.8% H_2 at 101 kPa.

B. *1-Hexene Hydrogenation*

Hexane was observed as a direct reaction product from 1-hexene along with appreciable amounts of the isomerization products *cis*- and *trans*-2-hexene as well as *cis*- and *trans*-3-hexene at higher conversions of 1-hexene. Because isomerization reactions are known to be catalyzed by acidic support materials, γ-Al_2O_3 and chlorinated γ-Al_2O_3 were also evaluated in separate reaction studies. Appreciable isomerization was noted with very little hydrogenation being found. For this reason, hexane production rates, extrapolated to zero conversion in 1-hexene, were used to discount isomerization activity of the support and the sulfided metal.

a. Kinetic models evaluated. Table 3 gives the kinetic parameters and residual sums of squares for the plausible 1-hexene hydrogenation rate equations obtained over 0.5% Ru/Al_2O_3 catalysts in the temperature range 548–608 K. Details of the kinetic results over 5% Ru/Al_2O_3 and $CoMo/Al_2O_3$ catalysts are given elsewhere (*22*).

As can be seen in Table 3, the most satisfactory correlation of the data for 1-hexene hydrogenation was found to be

$$-r_{Hx} = \frac{k_{Hx}P_{Hx}P_{H_2}}{(1 + K_{Hx}P_{Hx} + K_SP_S)^2} \qquad (2)$$

which is evidenced by the lower value of the residual sum of squares and the lower error bounds on the rate and the adsorption constants.

TABLE 3

Plausible Rate Models for 1-Hexene Hydrogenation[a]

Rate equation	T (K)	$k \times 10^6$ (mole/g · s · atm^2)	K_{Hx} (atm^{-1})	K_S (atm^{-1})	(Residual sum of squares)[b] $\times 10^{15}$
$\frac{kP_{Hx}P_H}{(1 + K_{Hx}P_{Hx})^2}$	548	1.01 ± 0.15	1.19 ± 0.97	—	0.53
	588	1.60 ± 0.27	1.05 ± 0.59	—	2.60
	608	2.48 ± 0.26	0.97 ± 0.66	—	2.04
$\frac{kP_{Hx}P_H}{(1 + K_{Hx}P_{Hx} + K_SP_S)}$	548	1.14 ± 0.16	3.21 ± 1.58	3.19 ± 2.30	0.62
	608	2.58 ± 0.26	2.32 ± 1.98	2.01 ± 1.28	2.13
$\frac{kP_{Hx}P_H}{(1 + K_{Hx}P_{Hx} + K_SP_S)^2}$	548	1.12 ± 0.08	1.57 ± 0.44	1.59 ± 0.45	0.33
	588	1.69 ± 0.16	1.30 ± 0.18	1.25 ± 0.24	2.42
	608	2.65 ± 0.13	1.19 ± 0.30	1.09 ± 0.32	1.40

[a] Based on 3.302 g of 0.5% Ru/Al_2O_3 in downflow quartz reactor, specimen (a) of Table 1.

[b] Obtained from the nonlinear least-squares regression analysis based on the method of Marquardt (*17*); residual sums of squares were determined by the differences between observed and computed rates.

The rate expression shown in Eq. (2) can be derived from two different reaction models. The first model is a two-site mechanism involving (i) competition between 1-hexene and hydrogen sulfide for the first site with adsorption of hydrogen at low coverage on the second site, (ii) two-point adsorption of 1-hexene, and (iii) surface reaction control. The second model is a single-site expression involving (i) competition between 1-hexene, hydrogen sulfide, *and* hydrogen for the site, (ii) one-point adsorption of 1-hexene, and (iii) surface reaction control.

Unfortunately, discrimination between the above models was not possible in this study since hydrogen served as the main constituent gas (viz., carrier gas) in the atmospheric reactor system and its partial pressure could only be varied over the range from 85.6 to 112.1 kPa. As such the influence of H_2 on the reaction rate could not be determined in sufficient detail to make a statistically significant choice between the above-noted models.

b. Results obtained from kinetic models. Kinetic and thermodynamic parameters obtained by fitting kinetic data to Eq. (2) are shown in Tables 4 and 5. It was observed (Table 4) that the adsorption constants for 1-hexene and H_2S are comparable on both Ru/Al_2O_3 and $CoMo/Al_2O_3$ catalysts, indicating about an equal inhibition of 1-hexene hydrogenation by 1-hexene and H_2S. In contrast to these results, Ramachandran and Massoth (*23*) found that 1-hexene hydrogenation rates over sulfided $CoMo/Al_2O_3$ were not inhibited by H_2S, although they pointed out that under the conditions of their study an explicit best equation could not be determined due to poor correlations between experimental data and model predictions.

Another notable trend provided by Table 5 is that the apparent activation energies for 1-hexene hydrogenation over sulfided Ru/Al_2O_3 catalysts decrease as ruthenium crystallite size is increased. Therefore, in order to examine in more detail the influence of surface structure on reaction rate, 1-hexene hydrogenation kinetics were also determined over reduced (i.e., sulfur-free) Ru/Al_2O_3 catalysts of varying crystallite size (see Fig. 3).

As expected, 1-hexene hydrogenation

TABLE 4

Fitted Kinetic Parameters under Various Reaction Conditions for 1-Hexene Hydrogenation[a]

Catalyst:	$CoMo/Al_2O_3$[b,c]			5% Ru/Al_2O_3[c,d]			0.5% Ru/Al_2O_3[c,e]		
T	$k \times 10^5$	K_{Hx}	K_S	$k \times 10^6$	K_{Hx}	K_S	$k \times 10^6$	K_{Hx}	K_S
548	4.33 ± 0.38	3.81 ± 0.70	1.25 ± 0.45	2.20 ± 0.16	3.25 ± 0.23	1.29 ± 0.25	1.12 ± 0.08	1.57 ± 0.44	1.59 ± 0.45
566	5.46 ± 0.85	2.87 ± 1.21	1.25 ± 0.50	—	—	—	—	—	—
588	6.28 ± 0.15	1.82 ± 1.20	1.25 ± 0.50	4.00 ± 0.23	2.28 ± 0.41	0.96 ± 0.37	1.69 ± 0.16	1.30 ± 0.18	1.25 ± 0.24
608	—	—	—	5.00 ± 0.32	1.94 ± 0.29	0.75 ± 0.21	2.65 ± 0.13	1.19 ± 0.30	1.09 ± 0.32

[a] Reaction model: $-r_{Hx} = kP_{Hx}P_{H_2}/(1 + K_{Hx}P_{Hx} + K_SP_S)^2$ (moles/g · s). Hx, 1-hexene; H_2, hydrogen; S, hydrogen sulfide; k, rate constant (moles/g · s · atm^2) determined from the above rate expression; this value is equal to the intrinsic rate constant (k^0) times $K_{H_2}K_{Hx}$. K_i, adsorption equilibrium constant for component i (atm^{-1}).

[b] Based on 0.04 g of $CoMo/Al_2O_3$ in tubular reactor.

[c] Presulfidization in 10% H_2S/H_2 at 673 K for 2 h.

[d] Based on 0.86 g of 5% Ru/Al_2O_3 in downflow quartz reactor, specimen (a) of Table 1.

[e] Based on 3.302 g of 0.5% Ru/Al_2O_3 in downflow quartz reactor, specimen (a) of Table 1.

over "clean ruthenium" surfaces appears independent of ruthenium dispersion, in agreement with the work of Benesi *et al.* (*24*) over Pt/SiO_2 catalysts and the expected facile nature of this reaction suggested by Boudart (*25*). Following sulfidization, however, the specific rate for 1-hexene hydrogenation decreased by one to two orders of magnitude depending on crystallite size, with smaller crystallites retaining significantly more of their intrinsic activity than larger crystallites. The origin of this anomaly is unclear but indicates that either (i) adsorbed sulfur can force a structure-insensitive reaction to become more demanding or (ii) adsorbed sulfur provides a size-dependent poisoning mechanism with smaller crystallites being somewhat more tolerant.

Figure 4 demonstrates that when 1-hexene hydrogenation rates measured over

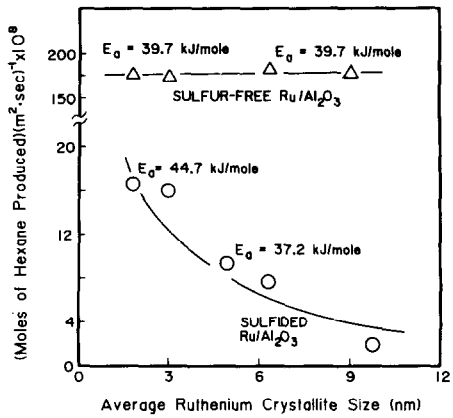

FIG. 3. 1-Hexene hydrogenation versus Ru crystallite size and presulfidization. Reaction conditions: (i) on sulfur-free specimens (prereduction in H_2, 101 kPa, 673 K, 8 h), data collected at P_{H_2} = 105.05 kPa, P_{Hx} = 6.97 kPa, 588 K; (ii) on sulfided specimens (same prereduction as noted above followed by sulfidization in 10% H_2S/H_2, 101 kPa, 673 K, 2 h), data collected at P_{H_2} = 105.04 kPa, P_{Hx} = 6.97 kPa, P_{H_2S} = 1.06 kPa, 588 K. Apparent activation energies determined from ln (global rate) versus $1/T$ over the temperature range from 548 to 608 K. Average crystallite size determined by H_2 chemisorption at 373 K prior to sulfidization.

TABLE 5

Kinetic and Thermodynamic Quantitites for 1-Hexene Hydrogenation versus Crystallite Size

Reference	Catalyst	d[a] (nm)	E[b] (kJ/mole)	ΔH_{Hx}[c] (kJ/mole)	ΔH_S[d] (kJ/mole)
(*35*)	$CoMo/Al_2O_3$	—	13.4[e]	17.8[e]	−148.4[e]
This work	$CoMo/Al_2O_3$	—	25 ± 8	−50 ± 8	0.0
This work	0.5% Ru/Al_2O_3	1.8	45 ± 10	−13 ± 1	−18 ± 2
This work	2% Ru/Al_2O_3	3.0	44 ± 2	—	—
This work	5% Ru/Al_2O_3	5.0	37 ± 3	−24 ± 1	−27 ± 9
This work	2% Ru/Al_2O_3	9.8	27 ± 5	—	—

[a] Average crystallite size determined by H_2 chemisorption before sulfidization (*5*, *6*).

[b] Apparent activation energy based on plot of ln (global rate) versus $1/T$.

[c] Heat of adsorption for 1-hexene based on van't Hoff plot of K_{Hx} versus $1/T$.

[d] Heat of adsorption for H_2S based on van't Hoff plot of K_S versus $1/T$.

[e] Quantities measured for butene hydrogenation.

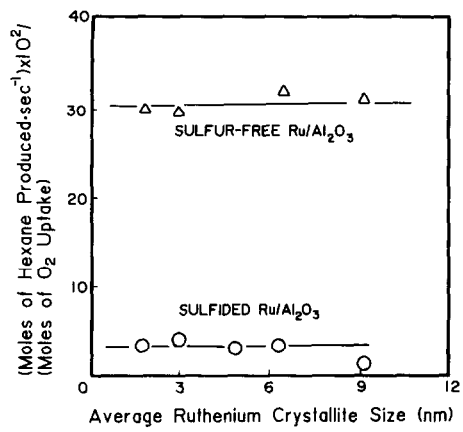

FIG. 4. 1-Hexene hydrogenation versus O_2 uptake over reduced and sulfided Ru/Al_2O_3 catalysts of varying crystallite size. Reaction conditions: (i) on sulfur-free specimens (prereduction in H_2, 101 kPa, 673 K, 8 h), data collected at P_{H_2} = 105.04 kPa, P_{Hx} = 6.97 kPa, 588 K; (ii) on sulfided specimens (same prereduction as noted above followed by sulfidization in 10% H_2S/H_2, 101 kPa, 673 K, 2 h), data collected at P_{H_2} = 105.04 kPa, P_{Hx} = 6.97 kPa, P_{H_2S} = 1.06 kPa, 588 K. Average crystallite size determined by H_2 chemisorption at 373 K prior to sulfidization. O_2 uptakes measured at 298 K following specified pretreatments.

the various catalysts used in this study are divided by their respective oxygen uptakes, corrected hydrogenation rates are obtained which are independent of ruthenium dispersion for both reduced and sulfided Ru/Al_2O_3 catalysts.

c. Hexene isomerization. Separate experiments investigating the isomerization of 1-hexene to *cis-* and *trans*-2-hexene were undertaken over ruthenium sponge catalysts before and after sulfidization and over a bulk RuS_2 specimen. Ruthenium sponge catalysts with surface areas of 6.5 m^2/g and unsupported RuS_2 catalysts with surface areas of 56 m^2/g were chosen to eliminate background isomerization activity provided by a support.

As shown in Table 6, specific isomerization rates increased following the indicated presulfidization treatments and kinetic evaluations in 1% H_2S, as compared to the reactivities observed over "sulfur-free" ruthenium sponges. Further increases in specific isomerization rates were also evident when bulk RuS_2 specimens were employed. Since sulfided ruthenium sponges are known to retain 0.25 monolayer of sulfur in a strongly bound state, with background H_2S competing for the remaining sites, the increase in activity following sulfidization suggests that the remaining ruthenium sites must possess relatively high isomerization activities.

Since sulfur is an electronegative adsorbate, partial monolayers adsorbed at a metal surface can create virtual cations of high Lewis acidity and increased isomerization activity (*26*). It is believed that such an explanation may account for the trends observed in Table 6. Additional evidence for these acid-type sites has recently been provided by other work in this laboratory which measured the carbon–oxygen stretching frequency of adsorbed carbon monoxide over supported Ru/Al_2O_3 catalysts in the presence and absence of adsorbed sulfur (*27, 28*). These studies, in agreement with similar efforts over Ni(111) (*29*) and Ni(100) (*30*), indicate that adsorbed sulfur can increase the stretching frequency of carbon monoxide consistent with a reduction in electron density at the remaining metal sites. Since increases in the acidity of the ruthenium surface may have a significant impact on the adsorption

TABLE 6

Isomerization Activity versus Sulfidization

Catalyst	Pretreatment	Moles of 2-hexene[a] produced per square meter per sec × 10^7
Ru sponge[b]	Reduction, 673 K, 8 h	3.6[c]
Ru sponge[b]	Reduction, 673 K, 8 h; presulfidization, 10% H_2S, 673 K, 2 h	5.2[d]
RuS_2[e]	Presulfidization, 10% H_2S/H_2, 673 K, 2 h	11.0[d]

[a] 2-Hexene identified by GC and NMR.
[b] Obtained from Engelhard; BET surface area, 6.5 m^2/g; > 96% purity.
[c] P_{H_2} = 105.04 kPa, P_{Hx-1} = 6.97 kPa, 588 K; H_2S not added to feed.
[d] P_{H_2} = 105.04 kPa, P_{Hx-1} = 6.97 kPa, P_{H_2S} = 1.06 kPa, 588 K.
[e] Prepared according to methods of Pecoraro and Chianelli (*1*); BET surface area, 56 m^2/g.

of Lewis bases such as thiophene, surface acidity may play a critical role in both thiophene activity and selectivity as discussed later.

C. Thiophene Hydrodesulfurization

Butane, butenes, and hydrogen sulfide were the primary reaction products under the conditions of this study using both Ru/Al_2O_3 and $CoMo/Al_2O_3$ catalysts. The distribution of desulfurized-C_4 products was observed in the following ranges: butane, 38.5–45.5%, and butenes, 54.5–61.5%, as determined at 588 K, P_{H_2} = 104.03 kPa, P_T = 10.34 kPa, and P_{H_2S} = 1.04 kPa. No butadiene was observed under any reaction conditions.

Since thiophene may react by two competing pathways which involve primary hydrogenolysis (R_I) or primary hydrogenation to tetrahydrothiophene (R_{II}) with rapid subsequent hydrogenolysis (R_{III}) (*31–33*), additional kinetic studies were required to verify that tetrahydrothiophene was not being produced as a primary product. Therefore, tetrahydrothiophene conversion was investigated separately to ensure that the measured kinetics for pathway R_{II} were not being obscured by rapid removal of the THT intermediate via reaction R_{III}. Results of these studies demonstrated that pathway R_{III}, while being about twice as fast as R_I, was nevertheless sufficiently slow so as to allow accurate determination of the R_I/R_{II} ratio in the limit of zero conversion. Mass balances involving the concentrations of hydrogen sulfide, thiophene, and tetrahydrothiophene in the reactant and product streams also verified that R_I was the only significant reaction pathway under the conditions of this study.

The absence of tetrahydrothiophene production in these studies over both $CoMo/Al_2O_3$ and Ru/Al_2O_3 catalysts is not unsual as similar investigations over MoS_2 (*34*) and $CoMo/Al_2O_3$ (*35*) detect little or no THT at hydrogen partial pressures of ca. 17 and 55–99 kPa, respectively, while other studies over WS_2 (*34*), RuS_2 (*4*), and $CoMo/Al_2O_3$ (*33*) detect significant quantities of THT at hydrogen partial pressures in the range of 17, 101, and 222–1770 kPa, respectively.

a. Kinetic models evaluated. Table 7 lists the kinetic parameters and the residual sums of squares obtained for the indicated rate expressions when compared against measured rate data obtained using 0.5% Ru/Al_2O_3 catalysts. Details of the kinetic results over 5% Ru/Al_2O_3 and $CoMo/Al_2O_3$ catalysts are given elsewhere (*22*).

As shown in Table 7, the best rate expression found to describe thiophene HDS was

$$-r_T = \frac{kP_TP_{H_2}}{(1 + K_TP_T + K_SP_S)^2} \qquad (3)$$

which is evidenced by lower values of the residual sum of squares and lower error bounds on the rate and the adsorption constants.

This rate equation agrees with work of Satterfield and Roberts (*36*) and Morooka and Hamrin (*37*). Analogous to the kinetic studies for 1-hexene hydrogenation, this model is also consistent with either a one- (*39, 40*) or a two-site (*35, 36, 38*) model but discrimination between these two cases was not possible due to our inability to vary the hydrogen partial pressure over a sufficiently large range.

b. Results obtained from kinetic models. Results obtained by fitting the kinetic data of Table 7 to Eq. (3) are shown in Tables 8 and 9. As can be seen, quantities measured in this study over $CoMo/Al_2O_3$ catalysts including K_T, K_S, E_a, ΔH_T, and ΔH_S agree fairly well with values reported in the literature (*35–37, 39, 41*). One anomaly observed, however, appears to be a somewhat lower heat adsorption of thiophene on the 0.5% Ru/Al_2O_3.

Adsorption equilibrium constants shown in Table 8 demonstrate that fundamental differences exist in the catalytic behaviors of $CoMo/Al_2O_3$ and Ru/Al_2O_3 specimens. Adsorption equilibrium constants for thio-

TABLE 7

Plausible Rate Equations for Thiophene HDS[a]

Rate equation	T (K)	$k \times 10^8$ (mole/g · s · atm^2)	K_T (atm^{-1})	K_S (atm^{-1})	K_H (atm^{-1})	(Residual sum of squares)[b] $\times 10^{17}$
$\frac{kP_TP_H}{(1 + K_TP_T + K_SP_S)}$	543	6.00 ± 1.00	4.30 ± 2.30	9.10 ± 2.50	—	0.72
	588	26.0 ± 4.0	4.20 ± 2.00	4.84 ± 1.50	—	2.85
$\frac{kP_TP_H}{(1 + K_TP_T + K_SP_S)^2}$	543	6.00 ± 1.00	2.16 ± 0.92	4.52 ± 1.07	—	0.64
	588	26.0 ± 1.50	2.09 ± 0.41	2.42 ± 0.32	—	2.49
$\frac{kP_TP_H}{(1 + K_TP_T + K_SP_S)(1 + K_HP_H)}$	543	5.00 ± 8.00	8.78 ± 8.31	11.0 ± 8.90	−0.27 ± 0.72	0.64
	588	42.0 ± 21.0	8.91 ± 3.12	19.7 ± 8.40	0.11 ± 0.33	1.47
$\frac{kP_TP_H}{(1 + K_TP_T + K_SP_S)(1 + K_HP_H)^2}$	543	3.00 ± 1.10	0.19 ± 3.10	0.74 ± 2.45	−0.15 ± 0.68	1.26
	588	39.0 ± 14.0	9.60 ± 2.50	15.1 ± 5.60	0.02 ± 0.13	1.10
$\frac{kP_TP_H^2}{(1 + K_TP_T + K_SP_S)(1 + K_HP_H)^2}$	543	2.00 ± 3.00	0.67 ± 2.16	3.26 ± 1.42	−0.35 ± 0.37	0.65
	588	42.0 ± 22.0	10.0 ± 1.80	10.7 ± 7.60	0.07 ± 2.00	1.75

[a] Based on 16.0 g of 0.5% Ru/Al_2O_3 in downflow quartz reactor, specimen (a) of Table 1.

[b] Obtained from the nonlinear least-squares regression analysis based on the method of Marquardt (*17*); residual sums of squares were determined by the differences between observed and computed rates.

phene (K_T) over $CoMo/Al_2O_3$ are significantly higher than those found on Ru/Al_2O_3, whereas HDS rates over Ru/Al_2O_3 are more inhibited by H_2S adsorption than those over $CoMo/Al_2O_3$.

Comparison of the two Ru/Al_2O_3 catalysts shown in Table 8 also indicates that smaller ruthenium crystallites are less inhibited by adsorbed hydrogen sulfide. In this instance, the reduced inhibition by hydrogen sulfide and the lesser amounts of irreversibly bound sulfur retained by these catalysts (see Fig. 1) suggest that smaller ruthenium crystallites are more resistant to both static and dynamic sulfur poisoning.

Figure 5 illustrates how the intrinsic activity behavior for thiophene HDS varies with crystallite size over Ru/Al_2O_3 speci-

TABLE 8

Fitted Kinetic Parameters under Various Reaction Conditions for Thiophene Hydrodesulfurization[a]

Catalyst:	$CoMo/Al_2O_3$[b,c]			5% Ru/Al_2O_3[c,d]			0.5% Ru/Al_2O_3[c,e]		
T (K)	$k \times 10^5$	K_T	K_S	$k \times 10^7$	K_T	K_S	$k \times 10^8$	K_T	K_S
543	—	—	—	—	—	—	6.0 ± 1.0	2.16 ± 0.92	4.52 ± 1.07
548	1.17 ± 0.35	9.20 ± 1.21	1.11 ± 0.51	—	—	—	—	—	—
566	3.19 ± 0.25	7.20 ± 0.85	0.74 ± 0.18	2.00 ± 0.25	1.87 ± 0.30	10.20 ± 1.85	—	—	—
588	6.90 ± 0.48	5.47 ± 0.78	0.52 ± 0.22	3.60 ± 0.30	1.01 ± 0.29	8.19 ± 1.71	26.0 ± 1.5	2.09 ± 0.41	2.42 ± 0.32
613	—	—	—	5.10 ± 0.41	0.55 ± 0.23	6.56 ± 1.48	—	—	—

[a] Reaction model: $-r_T = kP_TP_{H2}/(1 + K_TP_T + K_SP_S)^2$ (moles/g · s). T, thiophene; H_2, hydrogen; S, hydrogen sulfide; k, rate constant (moles/g · s · atm^2) determined from the above rate expression; this value is equal to the intrinsic rate constant (k^0) times $K_{H_2}K_T$. K_i, adsorption equilibrium constant for component i (atm^{-1}).

[b] Based on 0.1 g of $CoMo/Al_2O_3$ in tubular reactor.

[c] Presulfidization in 10% H_2S/H_2 at 673 K for 2 h.

[d] Based on 3.03 g of 5%/Ru/Al_2O_3 in downflow quartz reactor, specimen (a) of Table 1.

[e] Based on 16.0 g of 0.5% Ru/Al_2O_3 in downflow quartz reactor, specimen (a) of Table 1.

TABLE 9

Kinetic and Thermodynamic Quantitites for Thiophene HDS versus Crystallite Size

Reference	Catalyst	d^a (nm)	E^b (kJ/mole)	ΔH_T^c (kJ/mole)	ΔH_S^d (kJ/mole)
(36)	$CoMo/Al_2O_3$	—	15.5[e]	−100.3	−79.4
(37)	$CoMo/Al_2O_3$	—	83.6	—	—
(35)	$CoMo/Al_2O_3$	—	49.7	−51.0	−86.1
(39)	$CoMo/Al_2O_3$	—	104.5	—	—
(41)	$CoMo/Al_2O_3$	—	90.3	—	—
This work	$CoMo/Al_2O_3$	—	114 ± 15	−35 ± 1	−51 ± 7
This work	0.5% Ru/Al_2O_3	1.8	86.8	−2.1	−36.8
This work	2% Ru/Al_2O_3	3.0	76 ± 7	—	—
This work	5% Ru/Al_2O_3	5.0	58 ± 16	−75 ± 2	−27 ± 1
This work	2% Ru/Al_2O_3	9.8	53 ± 1	—	—

[a] Average crystallite size determined by H_2 chemisorption before sulfidization (5, 6).

[b] Apparent activation energy based on plot of ln (global rate) versus $1/T$.

[c] Heat of adsorption for thiophene based on van't Hoff plot of K_T versus $1/T$.

[d] Heat of adsorption for H_2S based on van't Hoff plot of K_S versus $1/T$.

[e] Mass transfer limitation (36).

mens. These data are displayed on two different bases. The first provides the moles of thiophene converted per square meter per second, as correlated on the basis of ruthenium surface areas measured by static hydrogen chemisorption prior to sulfidization. The second utilizes the moles of thiophene converted per second per mole of O_2 adsorbed, as correlated on the basis of pulse adsorption following presulfidization. Since both methods show marked increases in activity as crystallite size is reduced, they provide a clear indication of the structure-sensitive nature of thiophene HDS on sulfided Ru/Al_2O_3. Also, these trends cannot be ascribed to self-poisoning by either thiophene or hydrogen sulfide, as the respective adsorption equilibrium constants, when placed in Eq. (3), demonstrate that these species provide relatively little inhibition compared to the trends shown in Fig. 5.

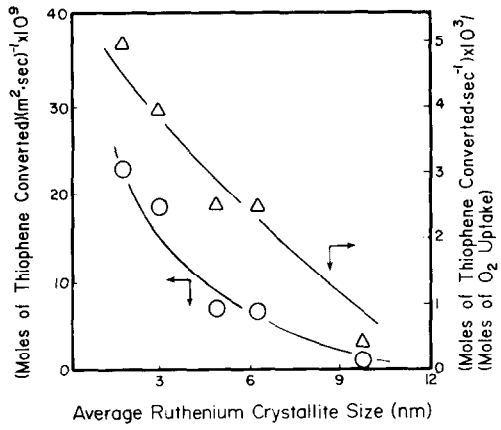

FIG. 5. Thiophene HDS versus Ru crystallite size. Catalysts presulfided in 10% H_2S/H_2, 101 kPa, 673 K, 2 h. Reaction conditions: P_{H_2} = 104.03 kPa, P_T = 10.34 kPa, P_{H_2S} = 1.04 kPa, 588 K. Average crystallite size determined by H_2 chemisorption at 373 K prior to sulfidization. O_2 uptakes measured at 298 K following sulfidization.

D. *Hydrodesulfurization/Hydrogenation Activity Ratios*

Figure 6 compares thiophene HDS to 1-hexene hydrogenation ratios at 548, 588, and 623 K for the single $CoMo/Al_2O_3$ catalyst investigated as well as for a number of the sulfided Ru/Al_2O_3 specimens of varying

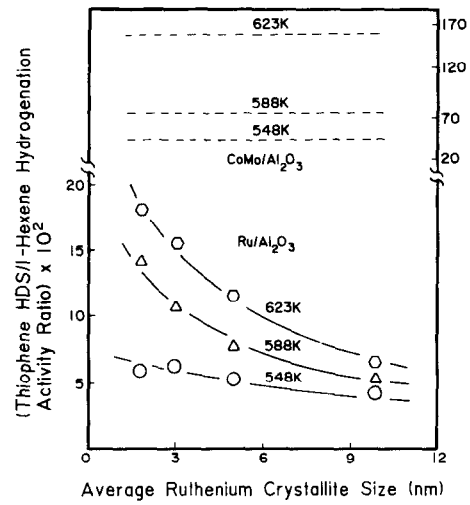

FIG. 6. Dependence of thiophene HDS/1-hexene hydrogenation activity ratio on Ru crystallite size at varying temperatures. Reaction conditions: P_{H_2} = 104.03 kPa, P_T = P_{Hx} = 10.34 kPa, P_{H_2S} = 1.04 kPa. Average Ru crystallite size determined by H_2 chemisorption at 373 K prior to sulfidization. Activity ratio for $CoMo/Al_2O_3$ not determined with respect to crystallite size.

crystallite size. In all cases, the HDS/hydrogenation ratio increased with increasing temperature, most likely as a result of the fact that apparent activation energies for HDS are greater than those for hydrogenation. Sulfided Ru/Al_2O_3 specimens possessed HDS/hydrogenation ratios that were 5 to 20 times lower than those for $CoMo/Al_2O_3$ catalysts depending on the temperature and ruthenium crystallite size employed. Of particular interest is the fact that on sulfided Ru/Al_2O_3 catalysts, the number of HDS reaction sites multiplied by the mean activity per site increases more rapidly with decreasing crystallite size than it does for 1-hexene hydrogenation. Thus, changes in the ruthenium crystallite size and the reaction temperature provide two distinct methods for tailoring the HDS-to-hydrogenation ratio over sulfided ruthenium catalysts within the inherent limits of this material. Additional ways to alter this ratio are discussed in Part II of this study (*4*).

DISCUSSION

1. Catalyst Characterization

A. *Micrograviметry*

Mild presulfidization of ruthenium sponge catalysts at 673 K in 101 kPa of 10% H_2S/H_2 provides stationary uptake ratios of ca. 0.3 ($S_{(a)}/Ru_{(s)}$ = 0.3). The amount of sulfur incorporated during identical sulfidization treatments, as monitored by X-ray photoelectron spectroscopy (*42*), indicates that sulfur adsorption is confined to the near or outermost surface region while X-ray diffraction (XRD) detected no apparent changes in the size or shape of the ruthenium crystallites. These results indicate that stable sulfur–ruthenium surfaces are generated following treatment in 10% H_2S/H_2 mixtures and points to the controlling influences provided by processes involving surface kinetics, bulk diffusion, and/or surface thermodynamics. Results of bulk thermodynamic calculations (*43*) predict formation of crystalline RuS_2 using H_2S/H_2 ratios as low as 2.69×10^{-5} at 673 K. It is this apparent region of "surface metastability" which provides the working surface for the kinetic studies reported in this paper while surfaces which incorporate more than 0.5 monolayer of sulfur are treated in Part II of this study (*4*).

Additional evidence for the region of "surface metastability" has been reported in the literature. Oliphant *et al.* (*44*) examined the chemisorption of hydrogen sulfide on 0.5% Ru/Al_2O_3 catalysts and found that the surfaces of these materials saturated at $S_{(a)}/Ru_{(s)}$ values of 0.4 following adsorption/reaction at temperatures as high as 723 K in 85 kPa of 30 ppm H_2S/H_2. Kelemen and Fischer (*45*) investigated the interaction of hydrogen sulfide with Ru (0001) using LEED, Auger electron spectroscopy (AES), and temperature-programmed desorption (TPD). They observed (2 × 2), $(\sqrt{3} \times \sqrt{3})R30°$, and c(4 × 2) LEED patterns, corresponding to surface coverages (i.e., $S_{(a)}/Ru_{(s)} = \theta_s$) of 0.25, 0.33, and 0.5, respectively, following treatments in 2–50 Langmuirs of H_2S at temperatures from 350 to 500 K. Agrawal *et al.* (*46*) observed sulfur coverages from 0 to 0.5 monolayer following adsorption/reaction in 101 kPa of 13–69 ppb H_2S during CO hydrogenation studies at 663 K. These results indicate that the maximum attainable *surface* coverage of sulfur is equal to one-half the number of surface ruthenium atoms. This saturation value most likely results from the specific site requirements for sulfur desorption and the larger van der Waals radii which sulfur posseses (i.e., S^0 = 0.185 nm, S^{-1} = 0.217 nm, and S^{-2} = 0.184 nm) compared to metallic ruthenium (Ru^0 = 0.133 nm).

B. *Chemisorption Studies*

As shown in Table 2, pulse oxygen uptakes over reduced Ru/Al_2O_3 catalysts are approximately one-half the value of the hydrogen uptake. In view of earlier discussions involving sulfur adatoms (*8–11*, *44–46*), this surface stoichiometry is not unexpected due to the site requirements for

oxygen adsorption and the somewhat larger van der Waals radii of oxygen than of ruthenium (i.e., O^0 = 0.140 nm, O^{-2} = 0.140 nm, Ru^0 = 0.133 nm). These data also indicate that (i) oxygen can be used to measure the surface areas of "clean" ruthenium surfaces and (ii) oxygen adsorption over "clean" ruthenium appears to be structure-insensitive over the diameter and temperature range examined in this study.

Following mild sulfidization in 101 kPa of 10% H_2S/H_2 at 673 K, a ca. 50% decrease in oxygen adsorption was observed over larger ruthenium crystallites (Fig. 1), which may correspond to one adsorbed sulfur atom for every four surface ruthenium atoms. This stoichiometry is consistent with earlier micrograviметric results from ruthenium catalysts which found sulfur coverages of ca. 0.3 monolayer following identical sulfidization treatments. The data of Fig. 1 thus suggest that crystallites greater than 3.2 nm are covered by ca. 0.25 monolayer of sulfur following sulfidization and become saturated by an additional 0.25 monolayer of oxygen following pulse adsorption.

The above-noted adsorption stoichiometries are consistent with the known saturation coverages of sulfur, at one sulfur adatom per two surface ruthenium atoms (*8–11, 44–46*) and the measured saturation coverages of oxygen, at one oxygen adatom per two surface ruthenium atoms (Table 2). Furthermore, since oxygen demonstrates no tendency toward structure sensitivity in the absence of sulfur, Fig. 1 suggests that the observed data are more indicative of a structure-sensitive adsorption by sulfur than by oxygen.

Evidence for structure-sensitive sulfur adsorption has been suggested by Bartholomew *et al.* (*47*) who indicate that sulfur possesses a tendency to preferentially adsorb at high coordination sites on any number of metal surfaces including Pt, Ag, Ru, Mo, Cu, Ni, Co, and Fe. Likewise, in a fashion similar to that of the above-noted oxygen chemisorption data, Gallezot *et al.* (*48*) found that smaller platinum crystallites were more resistant to sulfur poisoning. In the particular case of ruthenium, Kelemen and Fischer (*45*) found that 0.25 monolayer of sulfur form (2 × 2) LEED patterns with sulfur residing in high coordination threefold sites on the (0001) basal plane. The heat of desorption of sulfur was also found to be a strong function of coverage. Values as high as 439 kJ/mole were observed at coverages ≤0.25 monolayers, whereas values as low as 209 kJ/mole were observed as the surface neared saturation (i.e., θ_S = 0.5).

The enhanced stability exhibited by the (2 × 2) overlayer at θ_S = 0.25 may thus explain (i) the apparent quarter monolayer suppression in oxygen chemisorption noted over the large crystallites (Fig. 1) and (ii) the close to quarter monolayer of strongly adsorbed sulfur observed by micrograviметry. The tolerance of small crystallites toward sulfur poisoning may be rationalized on the basis that small crystallites, below 3.2 nm, possess relatively few high coordination sites, whereas crystallites greater than 3.2 nm are expected to provide larger fractions of the closest packing (0001) plane providing exactly one threefold adsorption site per surface ruthenium atom.

2. Kinetic Measurements

A. 1-Hexene Hydrogenation

a. Correlation of oxygen uptakes with 1-hexene hydrogenation before and after sulfidization. As demonstrated in Fig. 4, 1-hexene hydrogenation rates corrected by the oxygen uptake were independent of the ruthenium crystallite size. While these data suggest that 1-hexene hydrogenation is structure-insensitive, the fact that "sulfur-free" and "presulfided" catalyst systems fall on different horizontal lines, separated by an order of magnitude in specific reaction rate, is initially perplexing since earlier micrograviметric and oxygen chemisorption studies demonstrated that sulfided cat-

alysts possessed only 0.1–0.25 monolayer of irreversibly bound sulfur depending on crystallite size.

The above-noted dilemma can be rationalized, however, if it is recognized that sulfur interacts with the ruthenium surface in both a static and a dynamic fashion. Earlier noted microgravimetric and oxygen chemisorption experiments report the portion of the sulfur poisoning which is somewhat more static in nature and may be thought of as irreversibly adsorbed under the conditions of the adsorption studies. The data shown in Fig. 4, under the category of "sulfided Ru/Al_2O_3" specimens, however, were collected in the presence of ca. 1% H_2S, whereas studies involving "sulfur-free" Ru/Al_2O_3 had to be collected in the total absence of preadsorbed sulfur and background hydrogen sulfide. Therefore, the order of magnitude difference in apparent activities between the "sulfur-free" and "sulfided" specimens may be attributed to (i) inhibition by strongly bound sulfur adatoms which is most likely responsible for a 20 to 50% decline in activity based on the data shown in Fig. 1 and (ii) inhibition by competitively adsorbed H_2S which accounts for an additional fivefold decrease in activity.

Confirmations for the above-noted assignments to the overall activity decline were provided by the results of a separate experiment wherein a 2.0% Ru/Al_2O_3 specimen (3.0 nm) was evaluated at 588 K and under the conditions shown in Fig. 4. Following reduction in a sulfur-free environment, this catalyst provided a hexane yield equivalent to 57.9% conversion of the 1-hexene feedstream, whereas after addition of ca. 1% H_2S to the feedstream, the measured hexane production dropped over a period of 3 h to a stationary value of only 4.4% of the entering 1-hexene. While an initial conversion of 57.9% clearly places the reactor in a regime of nondifferential operation, the ca. tenfold decline in activity is consistent with the results shown in Fig. 4.

When hydrogen sulfide was removed from the feedstream the measured conversion to hexane increased to 13.6, 21.5, and 33.5% after 0.8, 5.0, and 17.0 h, respectively. This increase in activity could be hastened if the reaction temperature was increased, suggesting that removal of strongly bound sulfur species is facilitated at higher reduction/reaction temperatures. Results similar to these have also been observed over supported nickel catalysts during the hydrogenation of carbon monoxide (*49*).

The data of Fig. 4 thus suggest (i) that hexene hydrogenation is structure-insensitive under these conditions, (ii) that sites titrated by oxygen appear uniformly active, and (iii) that even though the data of Figs. 1 and 4 involve changes in both surface structure and poison levels, the reaction retains its structure-insensitive nature.

Despite the convincing evidence in support of a structure-insensitive mechanism, data shown in Table 5 and Fig. 3 still suggest that subtle differences exist over crystallites of different size. In particular, apparent activation energies and heats of adsorption for both 1-hexene and hydrogen sulfide (Table 5) show variations which are not observed in the case of studies conducted in the absence of sulfur (see Fig. 3). While explanations for this behavior are not available, it is known that measurements of lumped parameters such as the apparent activation energy also include the thermal dependencies of other parameters. These parameters include intrinsic activation energies and adsorption equilibrium constants, which involve the respective heats of adsorption for both reactants and poisons. In view of this realization, it is suggested that variations in both apparent activation energy and heat of adsorption versus crystallite size may be strongly influenced by variations in the thermal behavior of adsorbed hydrogen sulfide. Small variations in the thermal dependence of H_2S adsorption can have a significant impact on the observed conversion of 1-hexene since

H_2S and adsorbed sulfur dominate the reaction under these conditions.

b. Comparison of relative activities over Ru/Al_2O_3 and $CoMo/Al_2O_3$ catalysts. The relative activities of Ru/Al_3O_3 and $CoMo/Al_2O_3$ have been compared in Table 4 on a per gram of catalyst basis. It should be noted that this basis includes differences in both dispersion and loading and was employed since no consensus method currently exists for comparing the surface areas of sulfided $CoMo/Al_2O_3$ catalysts as recently discussed by Zmierczak *et al.* (*50*) and by Burch and Collins (*51*). Estimates for the intrinsic activities of these specimens can be made, however, based on (i) the results of oxygen chemisorption measurements performed after sulfidization and (ii) the metallic surface areas possessed by Ru/Al_2O_3 specimens prior to sulfidization (i.e., H_2 chemisorption) along with estimates for the dispersion of $CoMo/Al_2O_3$ catalysts. When making these types of activity comparisons it is important to note that neither RuS_2 nor Ru^0 (covered by partial monolayers of sulfur adatoms) form "layered structures" in the manner of MoS_2. So for this reason, specific activities have been reported, for convenience, using both methods.

Based on the first method noted above, it is found that division of the reaction rates computed from Table 3 by the measured oxygen uptakes shown in Table 2 provides values which indicate that the catalysts, 0.5% Ru/Al_2O_3, 5.0% Ru/Al_2O_3, and $CoMo/Al_2O_3$, possess relative activities of 0.035, 0.032, and 0.043 mole of hexane produced per mole of oxygen titratable sites per second at 588 K, respectively. Using the second approach noted above, it is found that 0.5% Ru/Al_2O_3, 5.0% Ru/Al_2O_3, and $CoMo/Al_2O_3$ catalysts possess relative activities of 0.16, 0.09, and 0.09 μmole of hexane produced per second per square meter at 588 K, respectively. This latter estimation procedure is based both on the number of surface metal atoms measured by hydrogen chemisorption procedures prior to sulfidization and on the assumption that 12% of the BET surface area of the $CoMo/Al_2O_3$ catalyst is composed of "active area." Since commercial $CoMo/Al_2O_3$ catalysts are known to provide significantly higher surface areas, which have been estimated at ca. 90% of the BET area (*52*), the above two estimation procedures indicate that sulfided 0.5% Ru/Al_2O_3 catalysts are about 13 times more active than $CoMo/Al_2O_3$ catalysts per square meter of "active surface area," while 1-hexene hydrogenation rates averaged over all sites titrated by pulse oxygen adsorption at 298 K are comparable.

B. Thiophene Hydrodesulfurization

a. Surface structure required for thiophene HDS. Data shown in Table 9 for thiophene HDS over Ru/Al_2O_3 are similar to those observed earlier for 1-hexene hydrogenation since apparent activation energies increase in both cases with decreasing crystallite size. Trends such as these generally suggest structure sensitivity, yet earlier discussions involving 1-hexene hydrogenation dismissed this explanation in view of convincing evidence provided to the contrary by oxygen chemisorption. In the particular case of 1-hexene hydrogenation, changes in the apparent activation energy were attributed to small variations in the thermal dependence of hydrogen sulfide adsorption versus crystallite size. While similar effects may be operative in the case of thiophene HDS, it is strongly suspected that this reaction should be more "demanding" in nature since it may involve cleavage of carbon–carbon bonds in the rate-determining step (i.e., hydrogenolysis) (*25*). In order to examine the structural requirements of this reaction in more detail, determinations of intrinsic activity versus crystallite size are discussed below.

The 23-fold increase in specific activity versus crystallite size observed in Fig. 5 cannot be attributed to just the number of sites blocked by strongly adsorbed sulfur as done in the case of 1-hexene hydro-

genation. Figure 1 and previously discussed microgravimetric data indicate that strongly bound sulfur coverages decrease from ca. 0.25 to 0.1 monolayer as the crystallite size is reduced from 3.2 to 1.8 nm. This decrease in sulfur coverage is insufficient for the observed increase in activity if a one-to-one site blockage occurs. Furthermore, specific rates based on the number of sites titrated by oxygen, which account for sites blocked by sulfur on a one-to-one basis, also indicate that small crystallites possess significantly higher activities (Fig. 5). While it is possible that larger ensemble requirements for thiophene HDS can magnify the presence or absence of sulfur poisons, the data obtained in this study involve simultaneous changes in surface structure and poison level which preclude ready calculation of an effective ensemble size.

Further examples of the influence of sulfur on the concentration of hydrogenolysis ensembles can be found in the noted increase in specific activity as ruthenium crystallite size is reduced. This trend is opposite to that observed for hydrogenolysis reactions on clean metals which indicate that closer packed planes, found in greater proportions on larger crystallites, are generally more active (*28, 53*). Thus, the observed activity trend over sulfided ruthenium appears to be dominated by *the absence of sulfur* and is similar in this regard to HDS studies over sulfided CoMo/Al_2O_3 catalysts which conclude that anion vacancies, found in high concentrations at MoS_2 edge planes, are mainly responsible for HDS activity (*54–58*). Massoth *et al.* (*59*) further examined this phenomenon by following the rate of thiophene HDS versus the size of MoS_2 crystallites supported on SiO_2–Al_2O_3. Their results, again unlike those for clean metals, noted increases in the intrinsic HDS activity as the crystallite size was reduced. Based on these results and surface area measurements/estimations provided by XRD, XPS, and oxygen chemisorption, Massoth *et al.* (*59*) suggested that dianion vacancies, found mainly at the corners of MoS_2 crystallites, are primarily responsible for HDS activity. The trends found by Massoth *et al.* (*59*) are thus quite similar to those observed in this study as the level of strongly adsorbed sulfur is reduced by decreasing the size of supported ruthenium crystallites.

b. Comparison of relative activities over Ru/Al_2O_3 and $CoMo/Al_2O_3$ catalysts. As with the earlier noted 1-hexene hydrogenation data, Table 8 compares the relative activities of Ru/Al_2O_3 and $CoMo/Al_2O_3$ on a basis which does not permit easy recognition as to which catalyst system possesses the highest intrinsic activity. If these two systems are compared on the basis of oxygen titratable sites, as described earlier, the relative activities of the 0.5% Ru/Al_2O_3, 5.0% Ru/Al_2O_3, and $CoMo/Al_2O_3$ catalysts are found to be 0.0049, 0.0025, and 0.034 mole of thiophene converted per second per mole of oxygen titratable sites at 588 K. Similar types of comparisons based on hydrogen adsorption measurements prior to sulfidization and estimates of the CoMo dispersion indicate that the relative activities of the 0.5% Ru/Al_2O_3, 5.0% Ru/Al_2O_3 and $CoMo/Al_2O_3$ catalysts are approximately 0.023, 0.0072, and 0.023 μmole of thiophene converted per second per square meter at 588 K, assuming that 38% of the BET surface area of the $CoMo/Al_2O_3$ catalyst is composed of "active surface area."

Since the active surface areas of CoMo/Al_2O_3 catalysts are generally regarded as being ca. 90% of the BET surface area (*52*), the above-noted estimation procedures indicate that 0.5% Ru/Al_2O_3 catalysts are about 2.4 times more active than CoMo/Al_2O_3 specimens per square meter of "active surface area," while thiophene HDS rates, averaged over all sites titrated by pulse oxygen adsorption at 298 K, are approximately 7 times larger over CoMo/Al_2O_3 catalysts than on 0.5% Ru/Al_2O_3 specimens. The disparity between the above two estimation procedures points toward the fact that differences exist in (i)

the number and potential activity of sites titrated by oxygen per square meter of "active surface area" on Ru/Al_2O_3 and $CoMo/Al_2O_3$ catalysts and (ii) the uniformity in activity per site titrated by oxygen over Ru/Al_2O_3 and $CoMo/Al_2O_3$ catalysts at fixed or varying dispersion levels. Indeed, evidence for the latter effect is provided by Fig. 5 which compares Ru/Al_2O_3 catalysts of various dispersions using the two above-noted estimation procedures.

SUMMARY/CONCLUSIONS

1. Mild presulfidization of ruthenium catalysts in 10% H_2S/H_2, 101 kPa, $T \leq 673$ K or in 100% of H_2S, 101 kPa, $T \leq 523$ K resulted in the formation of submonolayers of adsorbed sulfur ($S_{(a)}/Ru_{(s)} \leq 0.25$), which were evident from pulse oxygen chemisorption.

2. Sulfur coverages of ca. 0.1 monolayer were observed on 1.8-nm ruthenium crystallites compared to ca. 0.25 monolayer on $\geq$3.2-nm crystallites, indicating structure-sensitive adsorption of sulfur.

3. 1-Hexene hydrogenation over "clean" ruthenium surfaces appeared structure-insensitive. Following mild presulfidization specific rates decreased by one to two orders of magnitude depending on crystallite size. The anomalous structure sensitivity in 1-hexene hydrogenation noted above could be reconciled by counting sulfur-free ruthenium atoms using pulse oxygen chemisorption.

4. Increases in 1-hexene isomerization activity over sulfided ruthenium catalysts were attributed to the creation of virtual ruthenium cations of high Lewis acidity following adsorption of the electronegative adsorbate (sulfur).

5. Only direct C_4 hydrogenolysis products were observed during thiophene HDS over sulfided ruthenium catalysts. The specific rates of 1.8-nm crystallites were ca. 23 times greater than those of 10-nm crystallites. The higher specific activity of small ruthenium crystallites was attributed to the multiatomic ensemble requirements of the reaction, the higher activity associated with the "clean metal," and the greater number of "clean metal sites" on smaller crystallites.

6. Both 1-hexene hydrogenation and thiophene HDS over sulfided Ru/Al_2O_3 and $CoMo/Al_2O_3$ catalysts were well fit by Langmuir–Hinshelwood rate equations. Rates were inhibited by 1-hexene or thiophene and hydrogen sulfide. Apparent activation energies, adsorption equilibrium constants, and heats of adsorption were all found to depend on ruthenium crystallite size.

7. Sulfided Ru/Al_2O_3 (1.8-nm) catalysts provided ca. 13-fold higher 1-hexene hydrogenation rates than $CoMo/Al_2O_3$ catalysts when compared per square meter of active area, while specific 1-hexene hydrogenation rates were similar when compared per oxygen titratable site.

8. Sulfided Ru/Al_2O_3 (1.8-nm) catalysts provided ca. twofold higher thiophene HDS rates than $CoMo/Al_2O_3$ catalysts when compared per square meter of active area, while specific thiophene HDS rates were ca. sevenfold higher over $CoMo/Al_2O_3$ catalysts than over Ru/Al_2O_3 when compared per oxygen titratable site.

9. As a result of the above-noted activities, sulfided Ru/Al_2O_3 (1.8- to 10-nm) catalysts possesed ca. 5 to 20 times lower HDS/hydrogenation activity ratios than $CoMo/Al_2O_3$ depending on reaction conditions. This observation could be attributed to the difference of apparent activation energies between thiophene HDS and 1-hexene hydrogenation and the dependence of apparent activation energies on ruthenium crystallite size.

ACKNOWLEDGMENTS

Support for this work from the Department of Energy (DEAC 2283PC6044) and the Auburn University Engineering Experiment Station is acknowledged.

REFERENCES

1. Pecoraro, T. A., and Chianelli, R. R., *J. Catal.* **67**, 430 (1981).

2. Chianelli, R. R., *Catal. Rev. Sci. Eng.* **26,** 361 (1984).
3. Chianelli, R. R., Pecoraro, T. A., Halbert, T. R., Pan, W.-H., and Stiefel, E. I., *J. Catal.* **86,** 226 (1984).
4. Kuo, Y. J., and Tatarchuk, B. J., *J. Catal.* **112,** 250 (1988).
5. Lu, K., and Tatarchuk, B. J., *J. Catal.* **106,** 166 (1987).
6. Lu, K., and Tatarchuk, B. J., *J. Catal.* **106,** 176 (1987).
7. Kuo, Y. J., and Tatarchuk, B. J., Paper No. 13b, presented at the Symposium on Catalysts for Hydrotreating Heavy Crudes, Winter National Meeting of AIChE, Atlanta, GA, March 13, 1984.
8. Cocco, R. A., Toney, K. A., Kuo, Y. J., and Tatarchuk, B. J., Paper No. 88, presented at 190th National ACS Meeting, Division of Colloid and Surface Chemistry, Chicago, IL, Sept. 8, 1985.
9. Kuo, Y. J., Cocco, R. A., and Tatarchuk, B. J., Paper No. 34, presented at 191st ACS Meeting, Division of Petroleum Chemistry, New York, NY, April 13, 1986.
10. Kuo, J. J., Cocco, R. A., and Tatarchuk, B. J., "Petroleum Chemistry Preprints," p. 258. American Chemical Society, Washington, DC. Presented at 191st ACS Meeting, New York, NY, April 13, 1986.
11. Cocco, R. A., Kuo, Y. J., and Tatarchuk, B. J., presented at the Symposium on Energy-Related Fundamental Research in Kinetics and Catalysis, Winter National Meeting of AIChE, Miami, FL, November 2, 1986.
12. Lu, K., Kuo, Y. J., and Tatarchuk, B. J., submitted for publication.
13. Moran, D. L., M.S. thesis, Auburn University, 1985.
14. Bowers, D. E., M.S. thesis, Auburn University, 1987.
15. Dalla Betta, R. A., *J. Catal.* **34,** 57 (1974).
16. Goodwin, J. G., Jr., *J. Catal.* **68,** 227 (1981).
17. Marquardt, D. W., *J. Soc. Ind. Appl. Math.* **11,** 431 (1963).
18. Taylor, K. C., *J. Catal.* **38,** 299 (1975).
19. Gay, I. D., *J. Catal.* **80,** 231 (1983).
20. Satterfield, C. N., "Mass Transfer in Heterogeneous Catalysis." MIT Press, Cambridge, MA, 1970.
21. Mears, D. E., *Ind. Eng. Chem., Process. Des. Dev.* **10**(4), 541 (1971).
22. Kuo, Y. J., Ph.D. dissertation, Auburn University, 1987.
23. Ramachandran, R., and Massoth, F. E., *Chem. Eng. Commun.* **18,** 239 (1982).
24. Benesi, H. A., Curtis, R. M., and Studer, H. P., *J. Catal.* **10,** 328 (1968).
25. Boudart, M., "Advances in Catalysis" (D. D. Eley, P. W. Selwood, and P. B. Weisz, Eds.), Vol. 20, p. 153. Academic Press, San Diego, 1969.
26. Pines, H., "The Chemistry of Catalytic Hydrocarbon Conversions." Academic Press, New York, 1981.
27. Toney, K. A., M. S. thesis, Auburn University, 1985.
28. Kuo, Y. J., Heise, W. H., and Tatarchuk, B. J., submitted for publication; Kuo, Y. J., Heise, W. H., and Tatarchuk, B. J., presented at 193rd National ACS Meeting, Division of Colloid and Surface Chemistry, Denver, CO, April 5, 1987.
29. Trenary, M., Uram, K. J., and Yates, J. T., Jr., *Surf. Sci.* **157,** 512 (1982).
30. Gland, J. L., Madix, R. J., MacCabe, R. W., and DeMaggio, C., *Surf. Sci.* **143,** 46 (1984).
31. Mitchell, C. H., *Catalysis* **4,** 175 (1980).
32. Massoth, F. E., and Muralidhar, G., "Fourth Inter. Conf. Chemistry and Uses of Molybdenum." Climax Molybdenum Co., Golden, CO, 1982.
33. Devanneaux, J., and Maurin, J., *J. Catal.* **69,** 202 (1981).
34. Kieran, P. and Kemball, C., *J. Catal.* **4,** 394 (1965).
35. Lee, H. C., and Butt, J. B., *J. Catal.* **49,** 320 (1977).
36. Satterfield, C. N., and Roberts, G. W., *AIChE J.* **14,** 159 (1968).
37. Morooka, S., and Hamrin, C. E., Jr., *Amer. Chem. Soc.* **32,** 125 (1977).
38. Griffith, R. H., Marsh, J. D. F., and Newling, W. B. S., *Proc. R. Soc. London Ser. A* **197,** 194 (1949).
39. Desikan, P., and Amberg, C. H., *Canad. J. Chem.* **42,** 843 (1964).
40. Lipsch, J. M. J. G., and Schuit, G. C. A., *J. Catal.* **15,** 179 (1969).
41. Ozimek, B., and Radomyski, B., *Chem. Stoso.* **19,** 97 (1975).
42. Cocco, R. A., Kuo, Y. J, and Tatarchuk, B. J., in preparation.
43. McCarty, J. G., and Wise, H., *J. Chem. Phys.* **74**(10), 5877 (1981).
44. Oliphant, J. L., Fowler, R. W., Pannell, R. B., and Bartholomew, C. H., *J. Catal.* **51,** 229 (1978).
45. Kelemen, S. R., and Fischer, T. E., *Surf. Sci.* **87,** 53 (1979).
46. Agrawal, P. K., Katzer, J. R., and Manogue, W. H., *J. Catal.* **74,** 332 (1982).
47. Bartholomew, C. H., Agrawal, P. K., and Katzer, J. R., "Advances in Catalysis" (D. D. Eley, P. W. Selwood, and P. B. Weisz, Eds.), Vol. 31, p. 135. Academic press, San Diego, 1982.
48. Gallezot, P., Datka, J. Massardier, J., Primet, M., and Imelik, B., "Proceedings, 6th International Congress on Catalysis, London, 1976" (G. C. Bond, P. B. Wells, and F. C. Tomkins, Eds.), p. 696. The Chemical Society, London, 1976.
49. Fitzharris, W. D., Katzer, J. R., and Manogue, W. H., *J. Catal.* **76,** 369 (1982).

50. Zmierczak, W., Muralidhar, G., and Massoth, F. E., *J. Catal.* **77,** 432 (1982).
51. Burch, R., and Collins, A., *Appl. Catal.* **17,** 273 (1985).
52. Bodrero, T. A., and Bartholomew, C. H., *J. Catal.* **84,** 145 (1983).
53. Lam, Y. L., and Sinfelt, J. H., *J. Catal.* **42,** 319 (1976).
54. Tauster, S. J., and Riley, K. L., *J. Catal.* **67,** 250 (1981).
55. Tauster, S. J., and Riley, K. L., *J. Catal.* **70,** 230 (1981).
56. Bodrero, T. A., and Bartholomew, C. H., *J. Catal.* **78,** 253 (1982).
57. Bachelier, J., Duchet, J. C., and Cornet, D., *J. Phys. Chem.* **84,** 1925 (1980).
58. Topsøe, H., and Clausen, S. B., *Catal. Rev. Sci. Eng.* **26,** 395 (1984).
59. Massoth, F. E., Muralidhar, G., and Shabtai, J., *J. Catal.* **85,** 53 (1984).